

Not that long time ago in the nearest galaxy: 3D slice of molecular gas revealed by a 110 years old flare of Sgr A*.

E. Churazov,^{1,2} I. Khabibullin,^{1,2} R. Sunyaev,^{1,2} G. Ponti³

¹ *Max-Planck-Institut für Astrophysik, Karl-Schwarzschild-Strasse 1, 85741 Garching, Germany*

² *Space Research Institute (IKI), Profsoyuznaya 84/32, Moscow 117997, Russia*

³ *Max-Planck-Institut für extraterrestrische Physik, Giessenbachstrasse 1, Garching, 85748, Germany*

24 October 2016

ABSTRACT

A powerful outburst of X-ray radiation from the supermassive black hole Sgr A* at the center of the Milky Way is believed to be responsible for the illumination of molecular clouds in the central ~ 100 pc of the Galaxy (Sunyaev, Markevitch, & Pavlinsky 1993; Koyama et al. 1996). The reflected/reprocessed radiation comes to us with a delay corresponding to the light propagation time that depends on the 3D position of molecular clouds with respect to Sgr A*. We suggest a novel way of determining the age of the outburst and positions of the clouds by studying characteristic imprints left by the outburst in the spatial and time variations of the reflected emission. We estimated the age of the outburst that illuminates the Sgr A molecular complex to be ~ 110 yr. This estimate implies that we see the gas located ~ 10 pc further away from us than Sgr A*. If the Sgr B2 complex is also illuminated by the same outburst, then it is located ~ 130 pc closer than our Galactic Center. The outburst was short (less than a few years) and the total amount of emitted energy in X-rays is $\sim 10^{48} \rho_3^{-1}$ erg, where ρ_3 is the mean hydrogen density of the cloud complex in units of 10^3 cm^{-3} . Energetically, such fluence can be provided by a partial tidal disruption event or even by a capture of a planet. Further progress in more accurate positioning and timing of the outburst should be possible with future X-ray polarimetric observations and long-term systematic observations with Chandra and XMM-Newton. A few hundred-years long X-ray observations would provide a detailed 3D map of the gas density distribution in the central ~ 100 pc region.

Key words:

1 INTRODUCTION

While the luminosity of the supermassive black hole in the Milky Way is currently many orders of magnitudes lower than its Eddington limit (see, e.g., Genzel, Eisenhauer, & Gillessen 2010, for review), it is plausible that in the recent past the black hole was much more luminous (see Ponti et al. 2013, for review). In particular, a prominent spectral component, which is reminiscent of a spectrum formed when X-rays are “reflected” by cold gas, has been found from several molecular clouds within the central $\sim 1^\circ$ region around the Galactic center (e.g., Sunyaev, Markevitch, & Pavlinsky 1993; Koyama et al. 1996; Revnivtsev et al. 2004). Furthermore, the intensity of this reflected emission varies significantly on time scales of several years (e.g., Muno et

al. 2007; Koyama et al. 2008; Inui et al. 2009; Ponti et al. 2010; Terrier et al. 2010; Clavel et al. 2013), excluding the possibility that the observed emission is induced by a steady population of low energy cosmic rays, electrons or protons (see, e.g., Yusef-Zadeh, Law, & Wardle 2002; Tatischeff, Decourchelle, & Maurin 2012) interacting with molecular gas. A population of numerous persistent X-ray sources can also be excluded, since a large equivalent width of the neutral iron fluorescent line suggests that the primary emission is not contributing to the observed spectra. At present, the most plausible scenario assumes that an outburst (or several outbursts) of the Sgr A* emission few hundred years ago is responsible for the observed emission, although one cannot exclude another very bright transient source (or, several such

sources) as a culprit for individual clouds (see, e.g., Sunyaev et al. 1991; Churazov et al. 1993; Churazov, Gilfanov, & Sunyaev 1996; Sunyaev & Churazov 1998; Sunyaev, Gilfanov, & Churazov 1999). A number of observational and theoretical studies discuss possible ways of proving that primary radiation is indeed coming from Sgr A* and implications for the black hole past outbursts (see, e.g., recent studies Mori et al. 2015; Zhang et al. 2015; Molaro, Khatri, & Sunyaev 2016, and references therein).

Here, we compare spatial and temporal variations of the “reflected” flux to infer the time of the outburst and 3D positions of illuminated clouds. In §2, we describe the construction of reflected emission maps. We then use these maps to calculate the structure functions in space and time domains (§3), and infer the time of the outburst and 3D positions of illuminated clouds. The implications of our findings are discussed in §4. The final section summarizes our results.

Throughout the paper we assume the distance to Sgr A* of 8 kpc, 1' corresponds to 2.37 pc.

2 REFLECTION COMPONENT MAPS

In order to generate maps of reflected emission we follow the procedure described in Churazov et al. (2016). Briefly, we assume that the observed spectrum $S(E)$, in the energy band from 5 to 8 keV, can be described by a linear combination of two spectral templates:

$$S(E) = A_1 R(E) + A_2 P(E), \quad (1)$$

where, $R(E)$ and $P(E)$ are the template spectra for the reflected component and hot plasma emission, respectively, and A_1 and A_2 are free parameters of the model. For the hot plasma component $P(E)$, we use the APEC model (Smith et al. 2001) of an optically thin plasma emission with a temperature fixed to 6 keV. This component is merely a convenient way to capture the contribution of faint X-ray sources to the 5–8 keV band (Revnivtsev et al. 2009). For the reflected component $R(E)$, we have selected one of the simulated spectra of the reflected emission from Churazov et al. (2016). In these Monte-Carlo simulations a spherical homogeneous cloud is illuminated by a parallel beam of X-ray radiation with a power law spectrum and photon index ~ 2 . These models are characterized by the Thomson optical depth of the cloud τ_T and the scattering angle (primary source – cloud – observer). In the subsequent analysis, we use one of these models, corresponding to $\tau_T = 0.5$ and the scattering angle of 90° . Despite the simplicity of the model given by eq. (1), the direct fitting of the spectra, extracted from several representative regions, shows that the model captures essential signatures of the reflected component – 6.4 keV line and hard X-ray continuum and separates contributions of hot plasma and reflected components (see Churazov et al. 2016).

A linear nature of the spectral model given by eq. (1) permits to readily generate the maps of each component. Such an analysis has been done for Chandra and XMM-Newton observations of the Galactic Center region. As an illustration, Fig. 1 shows the maps of the reflected component averaged over 2000–2008 (left) and 2009–2015 (right)

observations with Chandra. The images have been adaptively smoothed to reduce the photon counting noise. The comparison of these two images shows very clearly that i) the reflected component has a clear spatial substructure and ii) on time scales on the order of 10 years, the substructure changes very strongly. This is consistent with previous findings (e.g., Munro et al. 2007; Ponti et al. 2010; Capelli et al. 2012; Clavel et al. 2013).

The question rises about the relation between spatial and temporal variations of the reflected component intensity. We address this question in the next section.

3 STRUCTURE FUNCTION IN SPATIAL AND TIME DOMAINS AND L.O.S. POSITIONS OF MOLECULAR CLOUDS

In order to study spatial and temporal variations, we used all publicly available XMM-Newton observations of the Sgr A* region. Compared to Chandra, XMM-Newton has larger FoV and more regular (in time) coverage of the GC region. Applying the procedure described in the previous section to individual XMM-Newton observations we got a set of reflection maps $I(\vec{x}, t)$, where $\vec{x} = (x, y)$ are the projected coordinates and t is the time of the observation. To characterize variations of the flux in time and space, we calculated the structure functions S , defined as

$$S_s(\Delta\vec{x}) = \langle [I(\vec{x}, t) - I(\vec{x} + \Delta\vec{x}, t)]^2 \rangle, \quad (2)$$

$$S_t(\Delta t) = \langle [I(\vec{x}, t) - I(\vec{x}, t + \Delta t)]^2 \rangle, \quad (3)$$

for the space and time domain respectively, where averaging is done over t and \vec{x} . The resulting structure functions are shown in Fig. 2 (left panel). The Poisson noise contribution has been removed from the plotted data points.

What can we learn from the comparison of S_s and S_t ? Let us first examine the relation between the structure function of the gas density distribution and the reflected flux structure functions.

Assuming that at energies above 5 keV, the gas is optically thin, i.e., optical depth $\tau \ll 1$, the observed reflected X-ray flux $I(\vec{x}, t)$ is

$$I(\vec{x}, t) \propto \int \rho(\vec{x}, z) \frac{f(\theta)}{r^2} L(t') dz, \quad (4)$$

where $\rho(\vec{x}, z)$ is the gas density, z – the coordinate along the line of sight, $r = (R^2 + z^2)^{1/2}$, $f(\theta)$ accounts for the angular dependence of the reflected emission on the scattering angle θ (for the fluorescent line alone $f(\theta) = \text{const} = 1/4\pi$), $L(t')$ is the luminosity of the primary source and

$$z = \frac{c}{2}(t - t') - \frac{R^2}{2c(t - t')}, \quad (5)$$

(see, e.g., Couderc 1939), where $R = |\vec{x}|$ is the projected distance from Sgr A*.

The sketch of the geometry is shown in Fig. 3. For known $\rho(\vec{x}, z)$ and $L(t')$ the value of $I(\vec{x}, t)$ can be readily calculated. The structure function includes averaging over many points, in space and time, and in order to predict it,

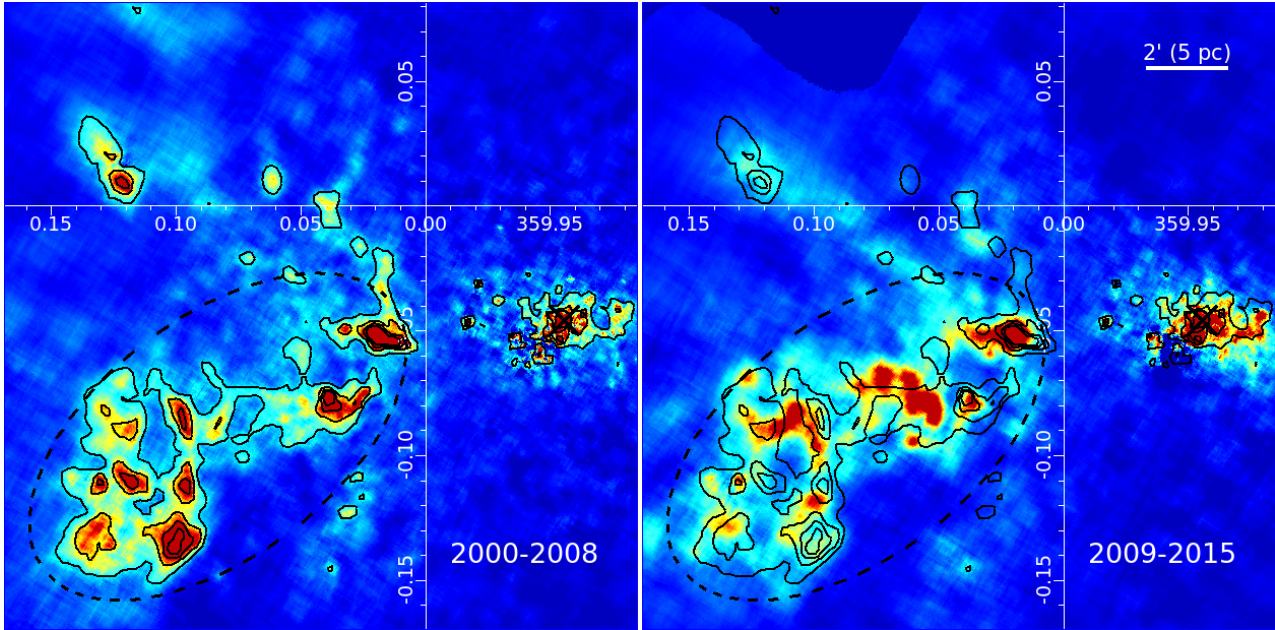


Figure 1. Comparison of Chandra images of the reflected emission averaged over 2000-2008 (left) and 2009-2015 (right) observations. The maps shown are in Galactic coordinates. It is clear that (i) there are significant spatial variations of the reflected flux and (ii) there are significant temporal variations on time scales of few years. The maps are based on spectral decomposition of the data in the 5-8 keV energy band into reflected and hot-plasma components [see eq. (1)]. The position of the Sgr A* is marked with a “cross”. The dashed line shows the area used for the structure function calculations. Below, we refer to this region as Sgr A complex. Note, that bright regions seen in the maps need not to be coherent structures in the velocity domain.

it is sufficient to know the power spectrum $P_I(k_x, k_y, k_t)$ of $I(\vec{x}, t)$, since $S(\vec{\Delta}) \propto \int P_I(k_x, k_y, k_t)(1 - \cos 2\pi\vec{\Delta}\vec{k})d^3k$. The power spectrum of $I(\vec{x}, t)$ can be found using eq. (4) via power spectra of ρ and L . For our purposes, it is convenient to consider a simplified version of eq. (4), assuming that i) we are dealing with a spatially small patch of the image centered at $\vec{x}_0 = (x_0, y_0)$ and ii) the outburst was short, i.e., we can set $L(t') = \Phi\delta(t' - t_0)$, where t_0 is the time when the outburst occurred and Φ is the total energy emitted. It is convenient to choose the coordinate system for this patch in such a way that x varies along the line connecting the primary source and the cloud, and y varies in the orthogonal direction, and $y_0 = 0$ chosen at the center of the patch, i.e., $R = x_0$, $r = \sqrt{x_0^2 + z_0^2}$. With these approximations one can assume that $\frac{f(\theta)}{r^2} \approx \text{const}$ and $I(\vec{x}, t) \propto \rho(\vec{x}, z)$, where z obeys eq. (5), substituting $t' = t_0$.

We now make one more important assumption that the structure function S_ρ of the density variations described by $\rho(\vec{x}, z)$ is isotropic in space on scales smaller than several pc¹. The relation between S_ρ and the measured structure

functions is as follows

$$\begin{aligned} S_t(\Delta t) &= AS_\rho \left(\Delta t \frac{\partial z}{\partial t} \right) \\ S_x(\Delta x) &= AS_\rho \left(\Delta x \sqrt{1 + \left(\frac{\partial z}{\partial x} \right)^2} \right) \\ S_y(\Delta y) &= AS_\rho(\Delta y), \end{aligned} \quad (6)$$

where A is a constant (same for all expressions) and

$$\begin{aligned} \frac{\partial z}{\partial t} &= \frac{c}{2} \left[1 + \left(\frac{x_0}{c(t - t_0)} \right)^2 \right] \\ \frac{\partial z}{\partial x} &= -\frac{x_0}{c(t - t_0)} \end{aligned} \quad (7)$$

The physical interpretation of eq. (6) is clear from Fig. 3: with time the locus of the illuminated points at a given (x, y) is moving in z direction at the velocity $\frac{\partial z}{\partial t}$. Thus, our measurements of time variations of the reflected flux are effectively probing variations of density along z . The variations of flux along x are affected by the inclination of the “paraboloid” to the picture plane, consequently, in projection we see clouds “squeezed” in this direction (see also §4 and Fig. 6 below). Finally, S_y is a direct probe of S_ρ .

From eq. (6) it is clear that by comparing structure functions in time and space domains, we can determine, e.g., the value of $\frac{\partial z}{\partial t}$, which in turn [see eq. (7)] relates x_0 and the time elapsed after the outburst. Since our spatial structure function has been calculated without making any dis-

¹ On large scales (larger than ~ 10 pc) this assumption is likely violated.

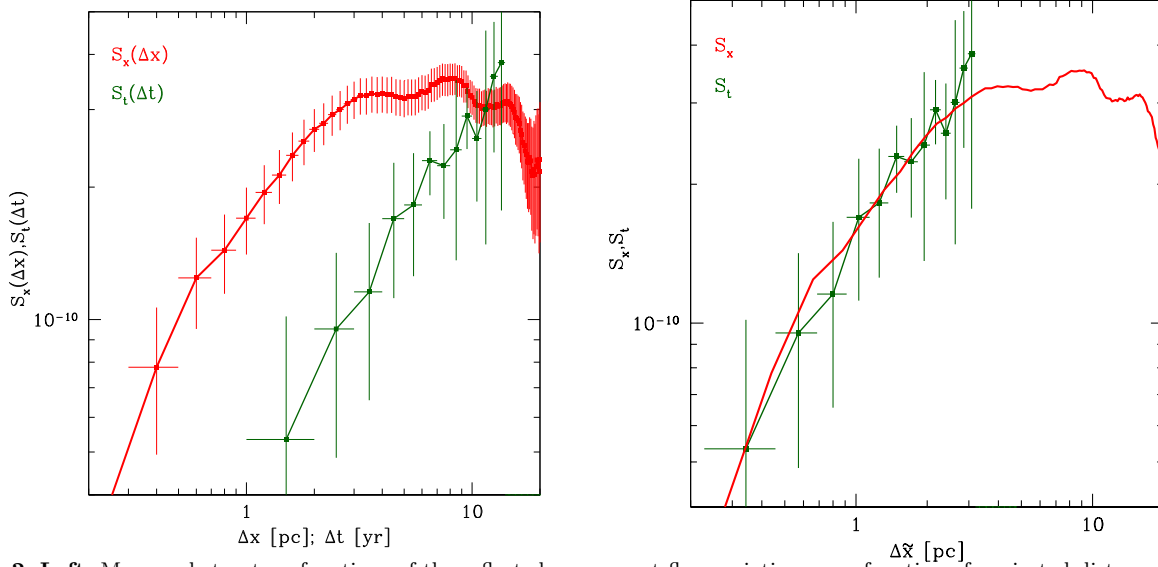


Figure 2. **Left:** Measured structure functions of the reflected component flux variations as a function of projected distance separation (red) and time (green). All publicly available XMM-Newton observations of the Sgr A complex were used. The measurements are done within the region shown in Fig. 1 with the dashed line. The expected Poisson noise contribution has been subtracted. In the reflection scenario the structure functions are not independent, but are closely related. If the clouds are illuminated by a short flare of X-ray emission from Sgr A*, then one can simply shift these function along the horizontal axis to infer the age of the outburst. **Right:** Comparison of the “shifted” time and space structure functions under assumption that there was a single and short outburst from Sgr A* about 110 years ago. Good agreement suggests that the data are consistent with this scenario. If correct, the short flare scenario predicts that the structure function in the time domain should flatten at $\Delta t \gtrsim 15 - 20$ yr to match the flattening of the spatial structure function. This prediction can be verified with future observations covering much longer period of time. At present the uncertainties on the structure function $S_t(\Delta t)$ at $\Delta t \sim 15$ yr are far too large to place meaningful constraints.

tinctions between x and y direction, we adopt a simplified expression for $S_s(\Delta)$:

$$S_s(\Delta) = AS_\rho \left(\Delta \left[\frac{1}{2} \sqrt{1 + \left(\frac{\partial z}{\partial x} \right)^2} + \frac{1}{2} \right] \right), \quad (8)$$

intermediate between S_x and S_y , given by eq. (6).

From eq. (6) it follows that spatial and time structure functions should coincide if they are plotted with respect to the effective $\tilde{\Delta}_x$, i.e.

$$\tilde{\Delta}_x = \Delta_x \frac{1}{2} \left[\sqrt{1 + \left(\frac{x_0}{c(t-t_0)} \right)^2} + 1 \right] \quad (9)$$

$$\tilde{\Delta}_x = \Delta_t \frac{c}{2} \left[1 + \left(\frac{x_0}{c(t-t_0)} \right)^2 \right] \quad (10)$$

for the space and time domain respectively. We now can search for the value of $\eta = \frac{x_0}{c(t-t_0)}$ that provides the best match between two structure functions. This exercise is illustrated in the right panel of Fig. 2. The best match is found for $\eta = 0.7$, adopting $x_0 \approx 10' \approx 27.3$ pc, implying that the outburst happened $t - t_0 \approx 110$ yr ago. Another immediate conclusion is that bright clouds are located $z \sim 10$ pc further away than Sgr A*.

Within ~ 8 pc from Sgr A* (in projection) there are two prominent molecular structures, the so-called 50 km s^{-1} and 20 km s^{-1} clouds. There is no evidence for bright

reflected emission from these clouds in the Chandra and XMM-Newton data. Coil & Ho (2000) suggested that these clouds are located within $z \pm 10$ pc, but on the opposite sides (along the line-of-sight) from Sgr A*. Since for a closer vicinity of Sgr A* the locus of illuminated gas is located at $z \sim 0.5c \times 110 \text{ yr} \sim 17$ pc, the flare scenario predicts that by now both clouds are not illuminated – consistent with X-ray data. The 50 km s^{-1} could have been bright ~ 35 yr ago (if located at $z = 10$ pc) or even earlier.

Experiments with other values of η have shown that the values of η between 0.65 and 0.8 provide similarly good match. The corresponding range of the $t - t_0$ is ~ 120 -95 yr. On the other hand, for a broader range of values, e.g., $\eta = 0.3$ or 1, there is a clear mismatch between the manipulated structure functions (see Fig. 4).

The above calculations were done assuming that the duration of the outburst t_b is infinitely small. One gets constraints on t_b directly from the structure functions, since at small separations in time the function $S_t(\tilde{\Delta}_x)$ should drop compared to $S_s(\tilde{\Delta}_x)$. However the difference between $S_t(\tilde{\Delta}_x)$ and $S_s(\tilde{\Delta}_x)$ will only be prominent if the duration of the outburst is significantly longer than the light propagation time of a typical cloud along the line of sight, i.e., $t_b \gtrsim l / \frac{\partial z}{\partial t}$, where l is the characteristic size of the cloud. In addition, the finite angular resolution of the XMM-Newton is expected to introduce by itself a drop of the $S_s(\tilde{\Delta}_x)$ at small separations. If we assume an effective angular reso-

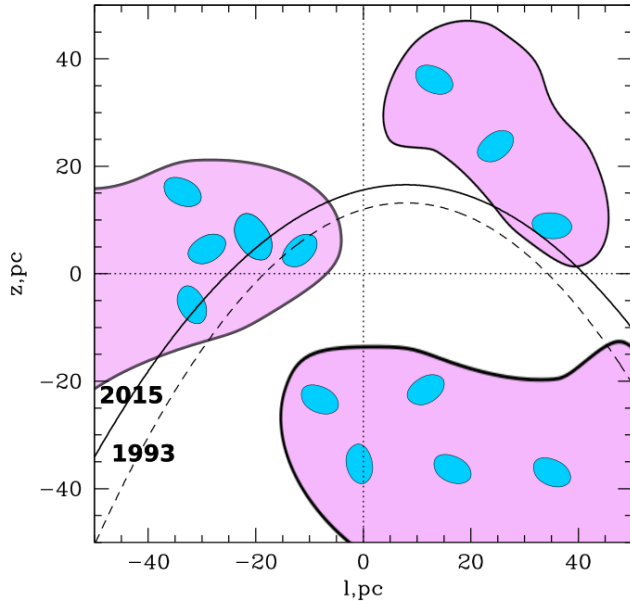


Figure 3. Sketch of a short outburst scenario for the outburst that happened ~ 110 years ago, assuming that the primary source is at (0,0). This is a view on the Galactic Center region from the Galactic pole, with the galactic longitude l along the horizontal axis, and the line of sight distance z along the vertical axis. The dashed and solid lines correspond to the position of the “light-front” in 1993 and 2015, respectively. The distance along the line of sight between the illuminated regions is given by $\sim \frac{\partial z}{\partial t}(t_2 - t_1)$, where $t_2 - t_1 \sim 22$ yr (see text). For regions close to primary source in projection, the value $\frac{\partial z}{\partial t} \sim 0.5c$. This value increases with projected distance from the primary source.

lution of $\sim 10''$, it translates into ~ 0.4 pc in space, or ~ 1.7 yr in time (assuming $\frac{\partial z}{\partial t} = 0.75c$). From Fig. 2 there is no evidence for a strong decline of S_s w.r.t. S_t . This suggests that the duration was shorter than a few years (see also Clavel et al. 2013). One can corroborate this conclusion by examining light curves of a few variable bright spots in the reflected emission maps (see Fig. 5). The light curves have been extracted from three regions. Regions 1 and 2 are located within the part of the Sgr A molecular complex that is bright in the reflected emission, while region 3 is a test region where reflected emission is faint. Corresponding light curves are shown in the right panel of Fig. 5. Red and black points correspond to XMM-Newton and Chandra observations, respectively. The flux is clearly variable with a peak in 2009–2010. The duration of the peaks sets an upper limit on the duration of the outburst. Even for an extremely short outburst the finite spatial extent of each cloud along the line of sight broadens the peak in the light-curves. For instance, for a cloud with the size of 1 pc, the minimum duration of the observed outburst, given $\frac{\partial z}{\partial t} \sim 0.75c$ is 4.3 yr. Based on this analysis, we have concluded that the assumption of a

short outburst [shorter than a few years; see also Clavel et al. (2013)] is reasonable.

4 DISCUSSION

The mean surface brightness of the reflected component in the analysed region (see Fig. 1) is $\sim 2 \cdot 10^{-5}$ phot cm $^{-2}$ s $^{-1}$ arcmin 2 in the 5–8 keV band. From this value (assuming fiducial parameters derived in the previous section and isotropic reflected emission) we can immediately estimate the total fluence $\Phi = L \times t_b$ of the primary source during the outburst

$$\Phi_{1-100 \text{ keV}} \sim 10^{48} \rho_3^{-1} \text{ erg}, \quad (11)$$

where ρ_3 is the mean gas density within the illuminated region in units of 10^3 cm^{-3} . The fluence in the 1–100 keV band was recalculated from the measured 5–8 keV flux assuming a photon index of 1.8, as estimated from INTEGRAL observations of the Sgr B2 cloud (Revnivtsev et al. 2004). Corresponding conversion factor is ~ 9.3 . For a photon index of 2 (see Terrier et al. 2010; Mori et al. 2015) this factor is ~ 9.8 . A fiducial value $\rho = 10^3 \text{ cm}^{-3}$ used in eq. (11) was motivated by the well studied Sgr B2 complex, where 10^3 cm^{-3} gas dominates the total mass budget on scales of tens of pc (Schmiedeke et al. 2016). The size of the region studied here (Fig. 1) is ~ 10 pc. Thus it seems reasonable to use the same fiducial value of density as in Sgr B2. The surface brightness in the studied region varies by a factor 10 (lower limit if small-scale substructure is present). Given our fiducial value of mean density, the brightest regions would correspond to local densities $\sim 10^4 \text{ cm}^{-3}$.

The luminosity, corresponding to the estimated fluence is

$$L_{1-100 \text{ keV}} \sim 5 \cdot 10^{40} \rho_3^{-1} \left(\frac{t_b}{1 \text{ yr}} \right)^{-1} \text{ erg s}^{-1}. \quad (12)$$

Note that in the *Nustar* study of the same region, Mori et al. (2015) suggested a much weaker limit on the Sgr A* luminosity $\gtrsim 10^{38} \text{ erg s}^{-1}$ in the 2–20 keV band. Apart from the factor of ~ 2 difference due to narrower energy band, the remaining difference is due to (i) the way the density/optical depth is defined and (ii) the assumed outburst duration. In Mori et al. (2015) the column density $N_H \sim 10^{23} \text{ cm}^{-2}$ of the reflected gas was estimated from the spectral modelling. For our fiducial value of $\frac{\partial z}{\partial t} \sim 0.75c$ and assumed duration of $t_b \sim 1$ yr, the required density is $N_H / (\frac{\partial z}{\partial t} t_b) \sim 10^5 \text{ cm}^{-3}$. The column density measurements from the spectra rely on the spectral distortions introduced by photoelectric absorption. However, if only a part of the cloud is illuminated, as it is the case when the flare is very short, the spectrally-derived column density corresponds to the characteristic column density of the entire cloud, rather than the column density of the illuminated gas. We therefore conclude that in the case of a short flare the column density (or mean density) that enters the conversion from the surface brightness to the luminosity of the primary source [see eq. (12)] does not necessarily coincide with the spectrally-determined column density. We therefore keep our scaling (via ρ_3) in all subsequent esti-

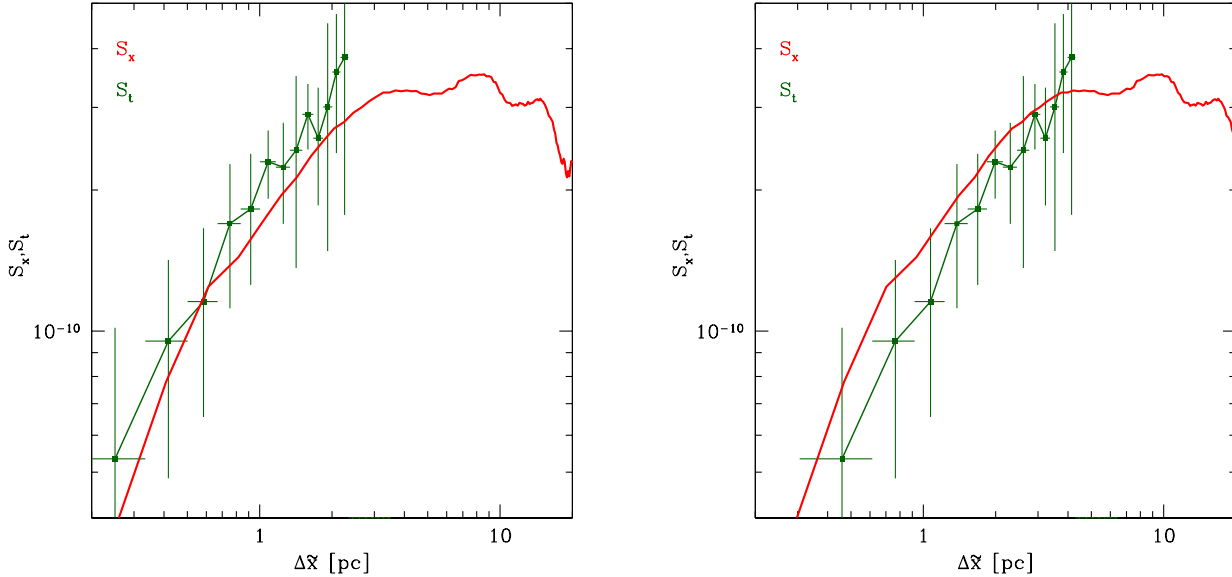


Figure 4. Same as in Fig. 2 for $\eta = 0.3$ (left) and $\eta = 1$ (right). In terms of elapsed time since the outburst the figures correspond to ~ 250 and ~ 75 yr respectively. Clearly the agreement between the structure functions is much poorer than for $\eta = 0.7$.

mates, but acknowledge that this value is uncertain by \sim one order of magnitude.

Based on Chandra observations of molecular clouds (similar region to the one studied here), Clavel et al. (2013) suggested that apart from a short (~ 2 yr long) flare that dominates the variability of some clouds, additional flares are responsible for the illumination of other clouds. This conclusion is primarily based on the comparison of the maximal fluxes from a set of clouds and the peak antenna temperatures in the CS and N_2H^+ lines for the same clouds. Clavel et al. (2013) found that the ratio of the X-ray and line fluxes differ among five clouds by a factor of ~ 6 . We believe that the uncertainties in association of X-ray peaks with the peaks from the position velocity cubes and conversion of molecular line fluxes to gas densities/column densities are large enough to allow for a single outburst scenario. We therefore keep the assumption of a single and short flare for the rest of the paper since it leads to the simplest picture. We note in passing that the structure functions can be explicitly expressed through the convolution of the gas density distribution power spectrum and the power spectrum of the flare. A short flare model, used here, has the advantage that most of the calculations are reduced to simple algebraic manipulations.

The minimal accreted mass, assuming high radiative efficiency at level of 10%, is $\delta M \sim \phi / (0.1c^2) \sim 10^{28} \rho_3^{-1} \text{ g} \sim 10^{-5} \rho_3^{-1} M_\odot \sim 10^{-2} \rho_3^{-1} M_J \approx 0.3 M_E$, where $M_J \approx 10^{-3} M_\odot$ and $M_E \approx 3 \times 10^{-6} M_\odot$ are Jupiter and Earth masses, respectively. Thus, this is a rather small value that can be easily provided by a tidal disruption (TDE) of a planet, or capture of the gas cloud similar to the one found by Gillessen et al. (2012). A scenario with a Jupiter-mass planet has been already considered in application to the past

Sgr A* activity by (Zubovas, Nayakshin, & Markoff 2012), but the predicted duration of a flare in this case is likely $\gtrsim 10$ yrs, while the actual frequency of such events is highly uncertain.

In order to produce a shorter flare one needs to disrupt a more massive body (having higher escape velocity), i.e. a super-Jupiter planet (see, e.g., Li, Narayan, & Menou 2002; Zubovas, Nayakshin, & Markoff 2012; Nikolaïuk & Walter 2013) or a star. The rate of “canonical” stellar TDEs is estimated at level $\sim \text{few} \times 10^{-5} \text{ yr}^{-1}$ per galaxy (van Velzen & Farrar 2014; Khabibullin & Sazonov 2014), while the peak luminosity of an associated flare can be as high as the Eddington limit for the SMBH (Rees 1988; Evans & Kochanek 1989; Ulmer 1999). However, the bulk of this radiation is likely to be in extreme UV and soft X-ray energy bands (Gezari et al. 2009; Komossa 2015), while hard X-ray emission is expected to originate from either a relativistic jet (Bloom et al. 2011; Burrows et al. 2011; Cenko et al. 2012) or a corona of hot electrons. In the former case, the hard X-ray emission should be beamed in the jet’s direction. Therefore, if viewed off-axis, the source can appear significantly dimmer. In the latter case, hard X-ray emission would also be rather dim due to the small optical thickness of the corona. Both of these opportunities still imply that the hard X-ray emission constitutes only a minor fraction of the event’s total energy output, and therefore some manifestations of its major contributor (i.e. soft X-ray emission, beamed X-ray emission or kinetic power of the jets) should be present (e.g. signatures of severe X-ray heating of the gas or jet-driven shocks). Still, some recent studies predict that a much smaller total radiative output might be more typical for TDEs (Piran et al. 2015), as a result of inefficient circularization of bound debris of the disrupted star.

All these scenarios remain speculative, given the uncertain, but in general low frequency of TDEs (see however Witzel et al. 2012, for discussion of a phenomenological model, extrapolating the Sgr A* flaring activity to rare, but very bright events).

If Sgr B2 is exposed to the same outburst, than it is located at $z \sim -130$ pc (closer to us than Sgr A*), and the velocity of the flare propagation along the line of sight is $\frac{\partial z}{\partial t} \sim 5c$ (for our fiducial parameters). The position estimate coincides with the value derived by Reid et al. (2009) based on the assumption that Sgr B2 is on the low eccentricity orbit around the Galactic Center. While the equality of two estimates is of course a coincidence, given the assumption and uncertainties, it is tempting to further examine this scenario. Firstly, one can consider this result as a confirmation that Sgr B2 is on the low eccentricity orbit. Secondly, we can directly compare the gas densities in the Sgr B2 cloud (and in any other cloud) relative to the Sgr A complex. The surface brightness of the reflected emission power by a short outburst is

$$I \propto \rho \frac{\partial z}{\partial t} r^{-2} \propto \rho \left[1 + \left(\frac{x}{c(t-t_0)} \right)^2 \right] [x^2 + z^2]^{-1}, \quad (13)$$

where z is related to x and $t-t_0$ according to eq. (5). Compared to the Sgr A complex, the decrease of the surface brightness due to r^{-2} term is partly compensated by the larger $\frac{\partial z}{\partial t}$ term ($\sim 5c$ for Sgr B2 compared to $\sim 0.75c$ for the Sgr A complex). During recent years, (e.g., 2012 observations of XMM-Newton), the mean surface brightness of the Sgr B2 region in the reflected emission was $\sim 5-6$ times lower than the mean surface brightness in the Sgr A complex (Fig. 1), which is consistent with the predictions. During earlier observations, e.g., before 2002, the two molecular complexes were almost equally bright, but this can be readily explained in the single-flare scenario if during these observations a denser part of the Sgr B2 complex was illuminated. Yet another constraint could come from the duration of the period when Sgr B2 was bright – at least for 24 years (from 1993 to 2015). Given that our fiducial value of $\frac{\partial z}{\partial t} \sim 5c$, this requires a size of $5c \times 24 \text{ yr} \approx 37$ pc along the line of sight. This is consistent with the size of the Sgr B2 cloud which according to Schmiedeke et al. (2016) is ~ 45 pc.

The best verification of the short flare scenario could come from the comparison of light curves from several compact cores in two molecular complexes at different projected distances from Sgr A* (e.g., Sgr B2 vs Sgr A complexes) – the shapes of the light curves should be similar once a correction on the factor $\frac{\partial z}{\partial t}$ is made. Another possibility is to use the difference between the spatial structure functions in the radial and tangential directions [see eq. (6)]. We illustrate this type of diagnostics in Fig. 6. The figure shows that when spherical clouds are illuminated by a short flare, they appear flattened in radial direction (reminiscent of weak lensing image distortions). The magnitude of this effect increases with the projected distance. Thus, such distortions (after averaging over many clouds) could be used to infer the position of the primary source [perpendicular to the squeezed direction] and the inclination of the paraboloid with respect to the picture plane [from the magnitude of distortions]. As discussed

in the previous section, the inclination is a proxy for the time of the outburst. One can also use the same approach to determine the duration of the flare – when the entire volume of a small cloud (smaller, than $\frac{\partial z}{\partial t} t_b$) is illuminated by the flare, the cloud should not appear as “squeezed” in radial direction, while larger clouds should.

Recently, several plausible models of the 3D distribution of molecular gas in the GC region have been suggested (e.g., Molinari et al. 2011; Kruijssen, Dale, & Longmore 2015; Henshaw et al. 2016). In these models a significant fraction of molecular gas is attributed to close or open orbits in the GC potential. One can use X-ray data to verify and calibrate these models. We simulate the expected reflected signal based on these models in another paper (Churazov et al. 2016). Here, we only note that in the most plausible model of Kruijssen, Dale, & Longmore (2015) the orbit passes some 50 pc behind Sgr A*. This implies that the reflected emission that we see in X-rays today is not associated with the clouds on this orbit. If an additional significant mass is indeed present along this part of the orbit, then the reflected signal from the same outburst should be seen hundreds of years later.

In this study, we have made a number of simplifying assumptions. Some of these simplifications can be avoided, but some are more fundamental. Among the latter is the assumption that the power spectrum of gas density fluctuations is isotropic. In reality, clouds might be preferentially stretched or squeezed in radial or tangential directions. A related problem is the finite number of clouds and/or strong correlation between the distribution of clouds in 3D. Most of the other simplifications can be avoided by doing more elaborate modelling based on eq. (4) that we defer to future work. A great deal of uncertainties can be removed by doing further observations. For instance, sufficiently long and regularly spaced in time (a few months) Chandra and XMM-Newton observations (preferably by the same telescope/detector configuration) would allow to measure the structure functions on small scales to better constrain the duration of the outburst and spatial structure function of illuminated clouds. Particularly powerful diagnostics would be possible with the detection of localized and transient spikes in the surface brightness, corresponding to small and dense cores of molecular clouds. Even more interesting would be to associate localized peaks in X-rays with maser sources, for which parallax measurements allow independent distance estimates.

Another extremely interesting possibility, is to use future polarimetric observations (see, e.g. Churazov, Sunyaev, & Sazonov 2002; Marin et al. 2015; Molaro, Khatri, & Sunyaev 2016) that can provide a direct measurement of the primary source position in the picture plane (from the polarization angle) and 3D position of the cloud (from the degree of polarization). For our fiducial parameters the scattering angle is $\sim 60^\circ$ for the bright part of the Sgr A complex, and the expected degree of polarization is close to 60%. The observed reflected flux from the entire ellipse (see Fig. 1) is $\sim 10^{-10} \text{ erg cm}^{-2} \text{ s}^{-1}$ in the 5-8 keV band. Even taking into account that i) fluorescent line emission is not polarized and ii) thermal plasma emission typically contributes about

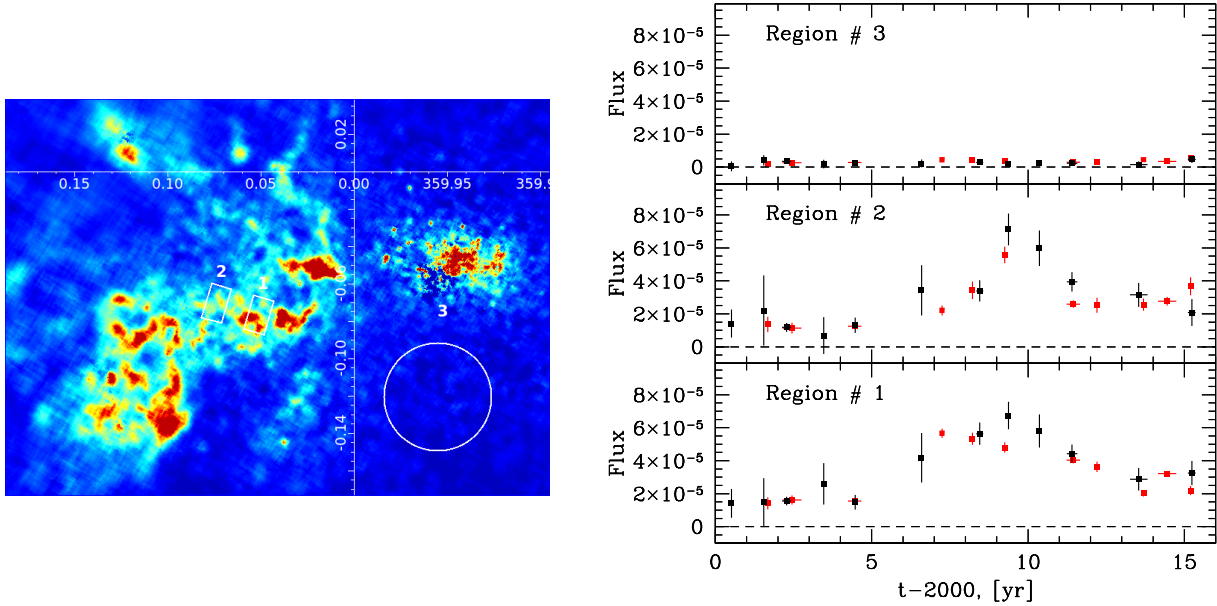


Figure 5. Light curves of reflected emission for selected regions. **Left:** Three regions used for the analysis, superposed onto Chandra map. Regions 1 and 2 are located within the molecular complex bright in reflected emission. Region 3 is a test region where reflected emission is faint. **Right:** Light curves for regions 1,2 and 3 (from bottom to top). Red and black points correspond to XMM-Newton and Chandra observations respectively. The duration of the peaks sets an upper limit on the duration of the outburst. Even for an extremely short outburst the finite spatial extent of each cloud along the line of sight broadens the peak. For instance, for a cloud with size of 1 pc, the minimum duration of the observed outburst, given $\frac{\partial z}{\partial t} \sim 0.75c$ is 4.3 yr.

half of the observed flux, it should be possible to detect polarization using future imaging polarimeters, e.g. XIPE (Soffitta et al. 2013) or IXPE (Weisskopf et al. 2013). The degree of polarization would be a solid proxy for the scattering angle. The same degree of polarization is expected for scattering by an angle θ and $\pi - \theta$. In reality, scattering smaller than 90° implies that the outburst happened less than $x0/c \sim 77$ yr ago. Even smaller angles can be effectively excluded, since it is unlikely that a powerful outburst from Sgr A* was missed by observers. Therefore, this ambiguity can be resolved.

The scenario described above opens an exciting perspective for accurate mapping of the molecular gas density in the GC region, once the fluence of the flare is reliably calibrated. Indeed, unlike any other method, the conversion factor from the surface brightness of reflected emission to the gas density is uncertain by a factor ~ 2 at most, due to the uncertainty in the iron abundance. All other gas properties like temperature, ionization state (as long as iron is not strongly ionized), molecular, atomic or dust grain phases do not make any significant difference to the conversion factor. An ambitious program of regular observations for **a few hundred!** years would effectively provide a full 3D picture of the molecular gas distribution over the entire 100 pc region. A “preview” (~ 3.4 pc thick) of a 3D gas distribution based on XMM-Newton observations is shown in Fig. 7. Moreover, once X-ray calorimeter data become available with future

observatories (like Athena, X-Ray Surveyor), this 3D mapping can be supplemented with gas velocity measurements unambiguously linking position-velocity data from molecular line observations with the 3D positions from X-ray data.

5 CONCLUSIONS

X-ray observations of the Galactic Center molecular clouds can serve as a powerful diagnostic tool for the 3D geometry of molecular gas and the past history of the Sgr A* activity. We used the comparison of spatial and temporal variations of the reflected emission flux to conclude that ~ 110 yr ago our supermassive black hole had a luminosity of the order of 10^{41} erg s $^{-1}$ over a period no longer than a few years. This conclusion implies that a molecular complex, currently exposed to Sgr A* radiation at ~ 20 pc from the source (in projection), is located ~ 10 pc further away than Sgr A* along the line of sight. We argue that these estimates can be further improved by future imaging and polarimetric observations. If there were only one or a few outbursts of Sgr A*, then it would eventually be possible to make a full 3D distribution of the molecular gas in the GC region.

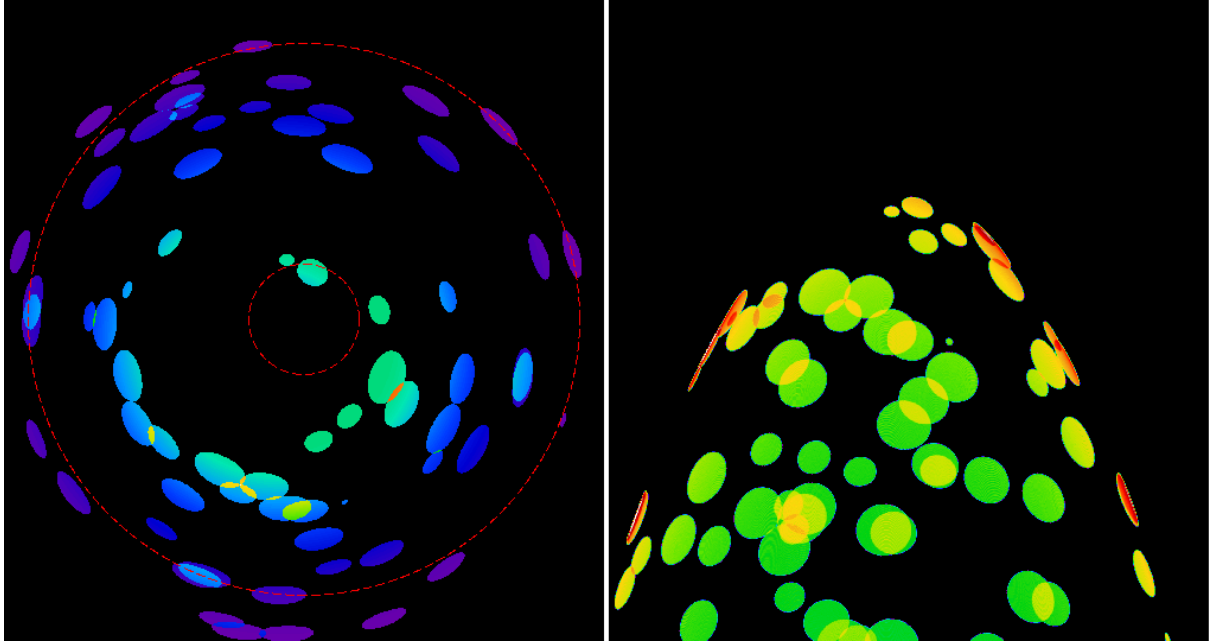


Figure 6. Apparent distortions of randomly distributed spherical clouds illuminated by a very short flare. In this illustration each cloud has a radius of 6 pc and a uniform density. The “paraboloid”, corresponding to the short flare, illuminates a thin slice in every cloud that it intersects. For a cloud at sufficiently large projected distance from the primary source, such a slice is inclined to the picture plane and in projection it looks flattened in the radial direction as shown in the left panel (see also Fig.3 in Sunyaev & Churazov 1998). The colors reflect the expected surface brightness of the clouds [see eq. (13)]. Two circles have the radii of 20 and 100 pc, approximately corresponding to Sgr A and Sgr B2 complexes, respectively. While the clouds look squeezed in radial direction, in tangential direction the clouds are not distorted. The analysis of such distortions can be used to infer the position of the primary source and the angle of the paraboloid with respect to the line of sight (or, equivalently, the time of the flare). The left panel shows a “side view” of the clouds that intersect with the paraboloid. Our fiducial value $t_b = 110$ yr is used.

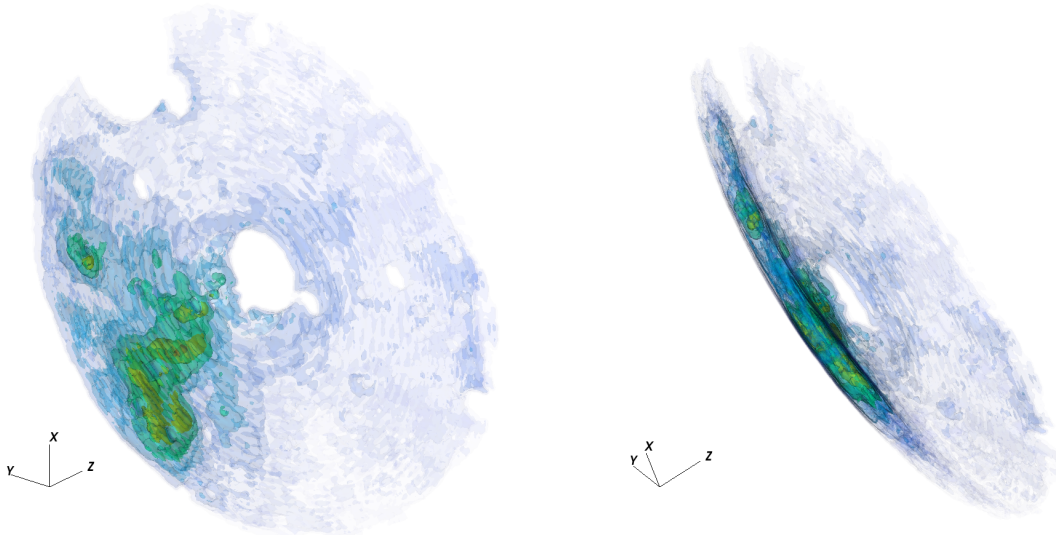


Figure 7. 3D distribution of gas near the Galactic Center based on our fiducial model of a short flare 110 years ago. The locus of the illuminated points at any given time is a paraboloid [see eq. (5)]. The surface brightness at location (l, b) observed by XMM-Newton at time t is recalculated to the gas density (scaled by a fiducial value of total fluence) and placed to a cell with coordinates (l, b, z) . The radius of the studied area is ~ 35 pc. The thickness of the paraboloid along the line of sight covered during ~ 15 yr of XMM-Newton observations is $\sim 0.75 \times c \times 15 \text{ yr} \approx 3.4$ pc. Left and right panels show different orientations of the same data cube. The “holes” correspond to excised regions contaminated by bright compact sources.

6 ACKNOWLEDGEMENTS

The results reported in this article are based in part on data obtained from the Chandra X-ray Observatory (NASA) Data Archive and from the Data Archive of XMM-Newton, an ESA science mission with instruments and contributions directly funded by ESA Member States and NASA. We acknowledge partial support by grant No. 14-22-00271 from the Russian Scientific Foundation.

REFERENCES

- Bloom J. S., et al., 2011, *Sci*, 333, 203
 Burrows D. N., et al., 2011, *Natur*, 476, 421
 Capelli R., Warwick R. S., Porquet D., Gillessen S., Predehl P., 2012, *A&A*, 545, A35
 Cenko S. B., et al., 2012, *ApJ*, 753, 77
 Churazov E., et al., 1993, *ApJ*, 407, 752
 Churazov E., Gilfanov M., Sunyaev R., 1996, *ApJ*, 464, L71
 Churazov E., Sunyaev R., Sazonov S., 2002, *MNRAS*, 330, 817
 Churazov E., et al., 2016, (in preparation)
 Clavel M., Terrier R., Goldwurm A., Morris M. R., Ponti G., Soldi S., Trap G., 2013, *A&A*, 558, A32
 Coil A. L., Ho P. T. P., 2000, *ApJ*, 533, 245
 Couderc P., 1939, *AnAp*, 2, 271
 Cramphorn C. K., Sunyaev R. A., 2002, *A&A*, 389, 252
 Evans C. R., Kochanek C. S., 1989, *ApJ*, 346, L13
 Genzel R., Eisenhauer F., Gillessen S., 2010, *RvMP*, 82, 3121
 Gezari S., et al., 2009, *ApJ*, 698, 1367
 Gillessen S., et al., 2012, *Nature*, 481, 51
 Henshaw J. D., et al., 2016, *MNRAS*, 457, 2675
 Inui T., Koyama K., Matsumoto H., Tsuru T. G., 2009, *PASJ*, 61, S241
 Khabibullin I., Sazonov S., 2014, *MNRAS*, 444, 1041
 Komossa S., 2015, *JHEAp*, 7, 148
 Koyama K., Maeda Y., Sonobe T., Takeshima T., Tanaka Y., Yamauchi S., 1996, *PASJ*, 48, 249
 Koyama K., Inui T., Matsumoto H., Tsuru T. G., 2008, *PASJ*, 60, S201
 Krolik J., Piran T., Svirski G., Cheng R. M., 2016, *arXiv*, arXiv:1602.02824
 Kruijssen J. M. D., Dale J. E., Longmore S. N., 2015, *MNRAS*, 447, 1059
 Li L.-X., Narayan R., Menou K., 2002, *ApJ*, 576, 753
 Marin F., Muleri F., Soffitta P., Karas V., Kunneriath D., 2015, *A&A*, 576, A19
 Molaro M., Khatri R., Sunyaev R. A., 2016, *A&A*, 589, A88
 Molinari S., et al., 2011, *ApJ*, 735, L33
 Mori K., et al., 2015, *ApJ*, 814, 94
 Munro M. P., Baganoff F. K., Brandt W. N., Park S., Morris M. R., 2007, *ApJ*, 656, L69
 Nikolajuk M., Walter R., 2013, *A&A*, 552, A75
 Piran T., Svirski G., Krolik J., Cheng R. M., Shiokawa H., 2015, *ApJ*, 806, 164
 Ponti G., Terrier R., Goldwurm A., Belanger G., Trap G., 2010, *ApJ*, 714, 732
 Ponti G., Morris M. R., Terrier R., Goldwurm A., 2013, *ASSP*, 34, 331
 Rees M. J., 1988, *Nature*, 333, 523
 Reid M. J., Menten K. M., Zheng X. W., Brunthaler A., Xu Y., 2009, *ApJ*, 705, 1548
 Revnivtsev M. G., et al., 2004, *A&A*, 425, L49
 Revnivtsev M., Sazonov S., Churazov E., Forman W., Vikhlinin A., Sunyaev R., 2009, *Nature*, 458, 1142
 Schmiedeke A., et al., 2016, *A&A*, 588, A143
 Smith R. K., Brickhouse N. S., Liedahl D. A., Raymond J. C., 2001, *ApJ*, 556, L91
 Soffitta P., et al., 2013, *ExA*, 36, 523
 Sunyaev R., et al., 1991, *ApJ*, 383, L49
 Sunyaev R. A., Markevitch M., Pavlinsky M., 1993, *ApJ*, 407, 606
 Sunyaev R., Churazov E., 1998, *MNRAS*, 297, 1279
 Sunyaev R., Gilfanov M., Churazov E., 1999, in Aschenbach B., Freyberg M. J., eds, *Highlights in x-ray astronomy*, MPE report No. 272, Garching, p. 120.
 Tatischeff V., Decourchelle A., Maurin G., 2012, *A&A*, 546, A88
 Terrier R., et al., 2010, *ApJ*, 719, 143
 Ulmer A., 1999, *ApJ*, 514, 180
 van Velzen S., Farrar G. R., 2014, *ApJ*, 792, 53
 Weisskopf M. C., et al., 2013, *SPIE*, 8859, 885908
 Witzel G., et al., 2012, *ApJS*, 203, 18
 Yusef-Zadeh F., Law C., Wardle M., 2002, *ApJ*, 568, L121
 Zhang S., et al., 2015, *ApJ*, 815, 132
 Zubovas K., Nayakshin S., Markoff S., 2012, *MNRAS*, 421, 1315